Korean J. Chem. Eng., 35(12), 2442-2451 (2018)
DOI: 10.1007/s11814-018-0156-z

pISSN: 0256-1115
eISSN: 1975-7220

Facile synthesis of $ZnBi_2O_4$-graphite composites as highly active visible-light photocatalyst for the mineralization of rhodamine B

Nguyen Thi Mai Tho*,**, Bui The Huy**,*******,†, Dang Nguyen Nha Khanh***, Ho Nguyen Nhat Ha***, Vu Quang Huy***, Ngo Thi Tuong Vy*****, Do Manh Huy******, Duong Phuoc Dat******, and Nguyen Thi Kim Phuong*,***,†**

*Graduate University of Science and Technology, Vietnam Academy of Science and Technology (VAST), 18 Hoang Quoc Viet, Cau Giay, Hanoi, Vietnam
**Institute of Research and Development, Duy Tan University, 03 Quang Trung, Da Nang, Vietnam
***HoChiMinh City Institute of Resources Geography, VAST, 01 Mac Dinh Chi, Ho Chi Minh City, Vietnam
****Chemical Engineering Faculty - Industrial University of Ho Chi Minh City, Vietnam
*****University of Science, National University of Ho Chi Minh City, Vietnam
******Institute of Chemical Technology, VAST, 01 Mac Dinh Chi, Ho Chi Minh City, Vietnam
*******Department of Chemistry, Changwon National University, Changwon 51140, Korea
(*Received 22 April 2018 • accepted 27 September 2018*)

Abstract−Novel highly active visible-light photocatalysts in the form of zinc bismuth oxide ($ZnBi_2O_4$) and graphite hybrid composites were prepared by coupling *via* a co-precipitation method followed by calcination at 450 °C. The as-prepared $ZnBi_2O_4$-graphite hybrid composites were tested for the degradation of rhodamine B (RhB) solutions under visible-light irradiation. The existence of strong electronic coupling between the two components within the $ZnBi_2O_4$-graphite heterostructure suppressed the photogenerated recombination of electrons and holes to a remarkable extent. The prepared composite exhibited excellent photocatalytic activity, leading to more than 93% of RhB degradation at an initial concentration of 50 $mg \cdot L^{-1}$ with 1.0 g catalyst per liter in 150 min. The excellent visible-light photocatalytic mineralization of $ZnBi_2O_4$-*1.0*graphite in comparison with pristine $ZnBi_2O_4$ could be attributed to synergetic effects, charge transfer between $ZnBi_2O_4$ and graphite, and the separation efficiency of the photogenerated electrons and holes. The photo-induced h^+ and the superoxide anion were the major active species responsible for the photodegradation process. The results demonstrate the feasibility of $ZnBi_2O_4$-*1.0*graphite as a potential heterogeneous photocatalyst for environmental remediation.

Keywords: Graphite, $ZnBi_2O_4$, Photocatalyst, Degradation, Mineralization

INTRODUCTION

Water-soluble organic dyes are one of the largest groups of pollutants in effluents from textile and other industries in a wide concentration range. It is well-known that conventional treatments (physical, chemical, and biological) are ineffective for removing many dye compounds because of their high stability and persistence. To address these issues, advanced oxidation processes (AOPs) such as photo-Fenton oxidation and photocatalytic oxidation have been developed and studied [1,2]. Heterogeneous photocatalysis is a promising method for the elimination of toxic and bio-resistant organic compounds by transforming them into innocuous species, and has been widely applied in the removal of organic pollutants in wastewater [2-4]. To date, heterogenous photocatalysis assisted by semiconductor oxides has proven to be an efficient and acceptable method for the purification of organic pollutants in aqueous media [2,5,6]. The construction of heterojunctions by coupling semiconductors with other semiconductors has become the most effective approach to improve the photocatalytic performance of catalysts [2,7-14]. Compared to a single component, heterojunction structures promote photocatalytic activity because of the synergistic effect, with benefits such as improved light absorption, increased charge transfer, and enhanced separation of photogenerated electron-hole pairs through the junctions at the interfaces [7,13,15-18].

Layered double hydroxides (LDHs), a group of layered functional materials with a special octahedral micro-structure, have the following major features: (i) the chemical composition of the layers is adjustable, (ii) the type and number of interlayer anions is exchangeable, and (iii) the particle size distribution can be controlled [19]. Recently, LDHs have received worldwide attention for their multiple applications as adsorbents [20-31], catalysts, and catalytic supports [32-44]. The general formula of LDHs is $[M_{1-x}^{2+} M_x^{3+} (OH)_2]^{x+} (A^{n-})_{x/n} \cdot yH_2O$, and they have been deemed to be the one of the most promising precursors of crystallized mixed metal oxides through calcination treatment [45]. Owing to their excellent visible-light-absorbing abilities, there have been numerous investigations of the application of LDH-based photocatalysts for the elimination of organic pollutants using artificial UV or solar

†To whom correspondence should be addressed.
E-mail: nguyenthikimp@yahoo.ca, buithehuy.nt@gmail.com

light as the irradiation source [2,42,46-48]. Among these photocatalysts, LDHs of the elements Ti, Bi, Zn, and Sn are preferred materials for photocatalytic processes [5]. However, most of them generally have a wide band gap and relatively high recombination rate of electron-hole pairs, with poor efficiency in terms of their photocatalytic activity.

Graphite is a carbon allotrope with a layered structure of stacked graphene sheets. It is commonly available and widely used as an adsorbent for organic pollutants because of its relatively low harmful effect on human health or the environment [49]. Several studies on the photocatalytic performance of graphite have been reported so far [50-53].

In the present work, ZnBi-LDH-*x*Graphite composites were obtained through a simple co-precipitation method, where *x* is the percentage of the graphite in the material. The prepared materials were then calcined at 450 °C to obtain the final composite consisting of ZnBi mixed-metal oxides and graphite-contained ZnBi mixed-metal oxides. The ZnBi-LDH-*x*Graphite composites were systematically investigated using various methods including field emission scanning microscopy (FESEM), X-ray powder diffraction (XRD) and UV-Vis spectroscopy. Graphite introduced in the composite served as a suitable conductor, increased the charge separation, and enhanced light absorption. The as-prepared ZnBi-LDH-*x*Graphite composites were applied for the photocatalytic degradation of hazardous organic contaminants (Rhodamine B). As expected, these ZnBi-LDH-*x*Graphite composites exhibited high photocatalytic activity and stability. Moreover, a mechanism to explain enhanced catalytic activity was proposed.

EXPERIMENTAL

1. Materials

All chemicals used were analytical grade. Bismuth(III) nitrate pentahydrate ($Bi(NO_3)_3{\cdot}5H_2O$) and sodium hydroxide (NaOH) were obtained from Junsei Chemical Co., Japan. Graphite, zinc(II) nitrate hexahydrate ($Zn(NO_3)_2{\cdot}6H_2O$), nitric acid (HNO_3), and rhodamine B were purchased from Sigma Aldrich.

2. Preparation of $ZnBi_2O_4$-*x*Graphite Composite

A typical synthetic procedure was as follows. A solution of graphite at different concentrations (*x*=0, 1, 2, 5, 10, and 20) was heated to 75±5 °C under magnetic stirring. Then, a solution of $Zn(NO_3)_2{\cdot}6H_2O$ and $Bi(NO_3)_3{\cdot}5H_2O$ in nitric acid (5%) with a molar ratio of 3 : 1 and an alkaline solution of 1 M NaOH were added dropwise at a flow rate of 2 mL/min. The pH value of the mixture was maintained at 10. The mixed solution was aged at 75±5 °C for 24 h. The materials obtained in this manner were subjected to centrifugation, washed, dried at 70 °C for 10 h, and then calcined at 450 °C for 3 h to obtain the Zn-Bi mixed-metal oxides ($ZnBi_2O_4$) and composites of $ZnBi_2O_4$ with graphite ($ZnBi_2O_4$-*x*Graphite). The as-prepared materials were labeled as $ZnBi_2O_4$, $ZnBi_2O_4$-*x*Graphite

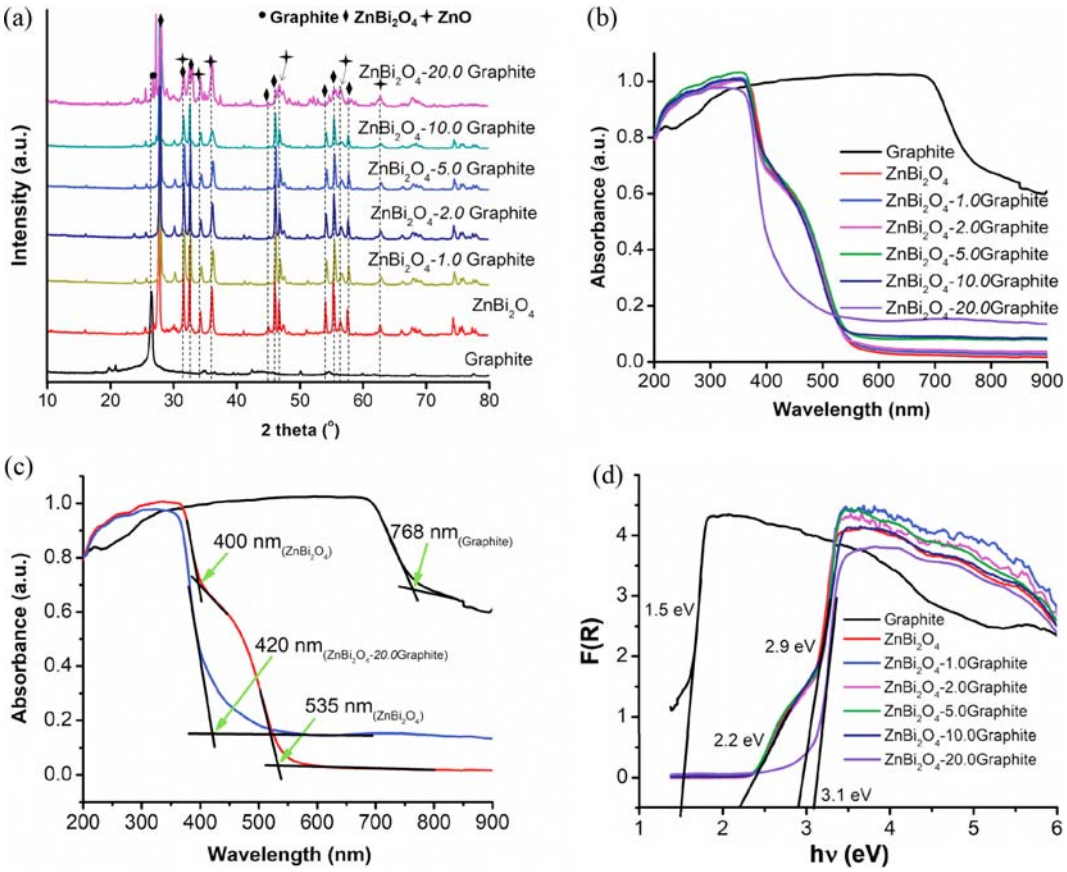

Fig. 1. (a) XRD patterns of the samples; (b) absorption spectra of $ZnBi_2O_4$ and $ZnBi_2O_4$-*x*Graphite (*x*=1, 2, 5, 10 and 20%), (c) the absorption edges of the samples, and (d) band gap energy of Graphite, $ZnBi_2O_4$, and $ZnBi_2O_4$-*x*Graphite composites.

(x=1, 2, 5, 10, and 20%) and hereafter will be referred to as $ZnBi_2O_4$, $ZnBi_2O_4$-*1.0*Graphite, $ZnBi_2O_4$-*2.0*Graphite, $ZnBi_2O_4$-*5.0*Graphite, $ZnBi_2O_4$-*10.0*Graphite, and $ZnBi_2O_4$-*20.0*Graphite.

3. Photocatalytic Experiments

The heterogeneous catalytic activities of the as-prepared materials were examined by measuring the degradation of RhB under visible-light irradiation. A 300 W halogen lamp (Osram, Germany) was used to provide a full spectrum emission without the use of a filter. For all experiments, the temperature of the reactor was maintained at 20 °C using circulating water. The suspension of the catalyst and RhB was stirred in a darkroom for 60 min to establish adsorption/desorption equilibrium, and then irradiated by turning on the halogen lamp. Five milliliters of the suspension was sampled at different time intervals (up to 150 min), and centrifuged to remove the catalyst. The quantity of RhB in solution was determined by measuring the UV-Vis absorption at a wavelength of 554 nm. The reactions were carried out in triplicate.

RESULTS AND DISCUSSION

1. Characterization of Materials

Generally, the incorporation of graphite in the $ZnBi_2O_4$ structure can be achieved by the simultaneous co-precipitation of graphite, Zn^{2+}, and Bi^{3+} in a NaOH solution followed by direct calcination at 450 °C in a muffle furnace. Fig. 1(a) shows the XRD patterns of graphite, $ZnBi_2O_4$, and $ZnBi_2O_4$-xGraphite. The XRD pattern of $ZnBi_2O_4$ shows several strong peaks at 2θ=27.8, 31.5, 32.8, 45.1, 46.0, 54.1, 55.4, and 57.5° corresponding to tetragonal zinc bismuth oxide (JCPDS No. 043-0449) and 31.5, 34.4, 36.1, 46.7, 57.5, and 62.8°, which represent the formation of pure hexagonal zinc oxide (JCPDS No. 079-0207). Almost all of the diffraction peaks are sharp and symmetrical, indicating good crystallinity. Pristine graphite typically shows a strong diffraction peak at around 26.6°. The diffraction pattern of $ZnBi_2O_4$-*20.0*Graphite is characterized by a new stronger peak at 27.3° as compared to that of pristine $ZnBi_2O_4$, indicating hybridization between graphite and $ZnBi_2O_4$. The main diffraction peaks of $ZnBi_2O_4$-xGraphite are similar to those of $ZnBi_2O_4$ and graphite.

The optical absorption of the as-prepared materials was measured using UV-Vis diffuse reflectance spectroscopy and the results are shown in Fig. 1(b). The pristine $ZnBi_2O_4$ material exhibits visible-light response with the absorption edges at 400 and 535 nm, indicating the presence of a small amount of the ZnO phase, while graphite shows intense absorption over the visible range that extends even to the infrared region (Fig. 1(c)). For the materials where 1-10% of graphite is composited with $ZnBi_2O_4$, the absorption edges are similar to that of $ZnBi_2O_4$ and blue-shifted in comparison with those of graphite. However, with increasing content of graphite up to 20%, the $ZnBi_2O_4$-Bi_2S_3 composites exhibit a mixed absorption at 420 nm. This change indicates a strong interaction between graph-

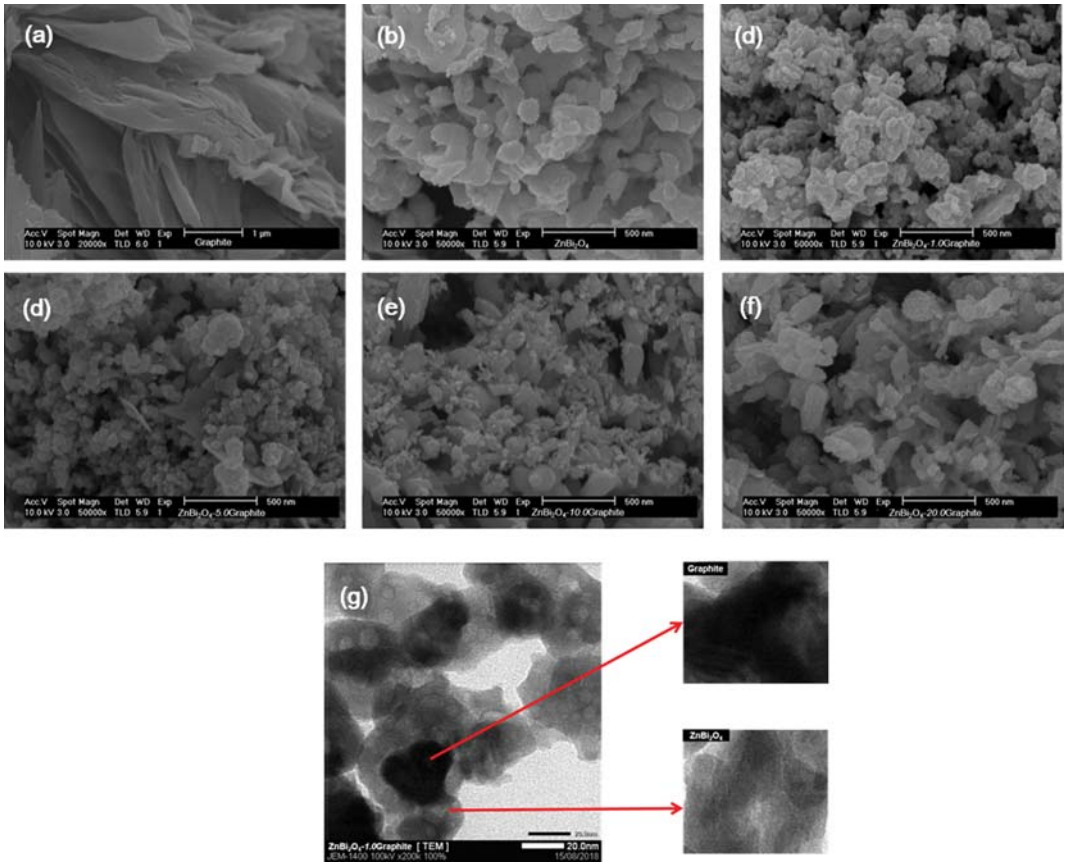

Fig. 2. SEM image of as-prepared samples (a) Graphite, (b) $ZnBi_2O_4$, and (c)-(f) $ZnBi_2O_4$-xGraphite (x=1, 5, 10 and 20%); (g) TEM image $ZnBi_2O_4$-*1.0*Graphite sample.

ite and $ZnBi_2O_4$ in the resulting $ZnBi_2O_4$-*x*Graphite photocatalysts, which strongly affects the light energy absorption region. The absorption spectra of $ZnBi_2O_4$-*x*Graphite extend to the visible-light region, indicating that these materials are visible-light responsive and their promising ability as photocatalysts under visible-light irradiation. A similar type of blue shift in absorption has also been observed for $ZnBi_2O_4$-gC_3N_4 [2], LDH/CdS nanofilms [40], and CN/NiFe composites [54].

The band gap energy (E_g) of the as-prepared materials was estimated using the Kubelka-Munk function and the results are shown in Fig. 1(d). It is well known that pristine ZnO has a large band gap energy (E_g=3.37 eV). In the present work, the band gap energy of the materials appeared at 2.9 eV indicating the presence of a ZnO impurity phase. Within the heterostructure of the ZnO impurity (E_g=2.9 eV) and $ZnBi_2O_4$ (E_g=2.2 eV), the conduction band (CB) and valence band (VB) potentials were calculated using the following formulas [8,12,55]:

$$E_{VB}=X-E^e+0.5\,E_g \quad (1)$$

$$E_{CB}=E_{VB}-E_g \quad (2)$$

where E_{VB} and E_{CB} are the VB and CB potentials, respectively, X is the electronegativity of catalysts and defined as the geometric mean of the absolute electronegativity of the constituent atoms (ca. 5.79 eV for ZnO and 6.11 eV for $ZnBi_2O_4$), and E^e is the energy of free electrons on the hydrogen scale (ca. 4.5 eV). The E_{VB} and E_{CB} values were approximately 2.74 and −0.16 eV for impurity ZnO; 2.71 and 0.51 eV for $ZnBi_2O_4$.

The morphologies of graphite, $ZnBi_2O_4$, and $ZnBi_2O_4$-*x*Graphite samples were investigated by SEM (Fig. 2). The SEM micrographs

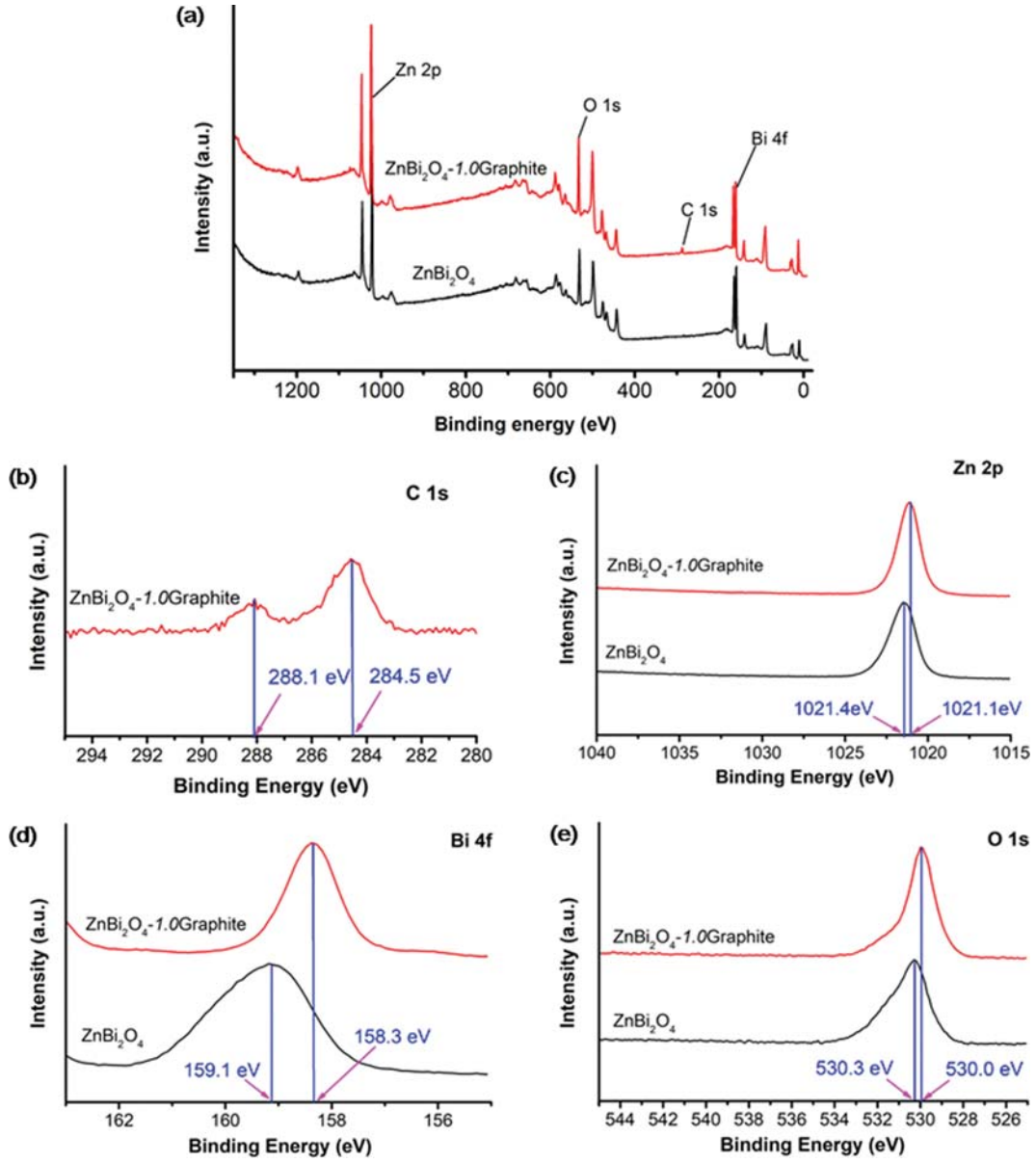

Fig. 3. XPS spectra of $ZnBi_2O_4$ and $ZnBi_2O_4$-*1.0*Graphite.

revealed that the as-prepared $ZnBi_2O_4$ consisted of irregularly stacked particles because of the collapse of the layered structure (Fig. 2(b)). The individual plates of $ZnBi_2O_4$ were flat and the edges of the plates appeared rounded. It is interesting that in case of $ZnBi_2O_4$-*x*Graphite samples, $ZnBi_2O_4$ tends to grow on the graphite sheet (Fig. 2(c)-2(f)). Fig. 2(g) shows the typical TEM images of the $ZnBi_2O_4$-*1.0*Graphite composite; it was found that the graphite sheets were densely covered by the $ZnBi_2O_4$ plates.

The interaction between the $ZnBi_2O_4$ and the graphite was investigated by X-ray photoelectron spectroscopy (XPS). The results of the XPS analysis of pristine $ZnBi_2O_4$ and $ZnBi_2O_4$-*1.0*Graphite samples are presented in Fig. 3. The C 1s XPS spectrum of graphite for the $ZnBi_2O_4$-*1.0*Graphite sample is shown in Fig. 3(b). A dominant peak at 284.4 eV and a weak peak at 288.1 eV are observed in the graphite spectrum corresponding to C-C (or C=C) and C=O, respectively [56]. A typical Zn 2p XPS spectrum in Fig. 3(c) exhibits the binding energy at 1021.4 eV for $ZnBi_2O_4$ sample. However, a shift of 0.3 eV to a lower binding energy of 1,021.1 eV is observed for $ZnBi_2O_4$-*1.0*Graphite sample. The binding energies of Bi 4f of $ZnBi_2O_4$-*1.0*Graphite sample exhibit a shift of 0.8 eV to lower binding energy compared with that of pristine $ZnBi_2O_4$. As shown in Fig. 3(d), the spectrum of Bi 4f shows a peak with binding energy of 159.1 eV for the $ZnBi_2O_4$ sample and 158.3 eV for the $ZnBi_2O_4$-*1.0*Graphite sample. The O 1s XPS spectrum of the $ZnBi_2O_4$ displays a peak centered at 530.3 eV. In the case of the $ZnBi_2O_4$-*1.0*Graphite sample, the shift of 0.3 eV to the lower binding energy of 530.0 eV is observed (Fig. 3(e)). The binding energies decreasing in the $ZnBi_2O_4$-*1.0*Graphite sample indicate an obvious charge transfer at the $ZnBi_2O_4$-*1.0*Graphite sample interface. The strong electronic coupling between $ZnBi_2O_4$ and graphite would likely accelerate the electron-hole separation.

2. Photocatalytic Activity

The dependence of RhB degradation on the graphite concentration in the catalyst was estimated by using different catalysts (100 mg catalyst/100 mL solution containing 50 mg/L of RhB at pH~2.0). The photocatalytic activity of the as-prepared catalysts was evaluated by measuring the degradation of RhB. Before irradiation, the dark adsorption equilibrium was established after 60 min. In the dark box for 60 min, ~12.8-25.7% RhB was adsorbed on the $ZnBi_2O_4$-*x*Graphite samples, while pristine $ZnBi_2O_4$ and graphite adsorbed 17.9 and 65.5% of RhB, respectively (Table S1). The removal of RhB using different as-prepared samples is shown in Fig. 4(a). As seen, the photolysis reaction also contributed to the degradation of RhB; 19% of RhB was degraded after 150 min of light exposure without a catalyst. After visible-light irradiation for 150 min, total RhB removal was 71.8% and 48.9% using graphite and $ZnBi_2O_4$, respectively. The efficiency of the RhB removal was further improved in the presence of $ZnBi_2O_4$-*x*Graphite (*x*=1, 2, 5, and 10%) composites as compared to that of $ZnBi_2O_4$, although $ZnBi_2O_4$-*20.0*Graphite had the least RhB removal efficiency. As seen in Table S1, total RhB removal using $ZnBi_2O_4$-*x*Graphite (*x*=1, 2, 5, and 10%) composites was in range of 56.6-93.8%, while $ZnBi_2O_4$-*20.0*Graphite removed about 33.8% of RhB. The $ZnBi_2O_4$-*1.0*Graphite composite exhibited the highest catalytic performance for RhB removal.

The total organic carbon (TOC) content in solution as well as

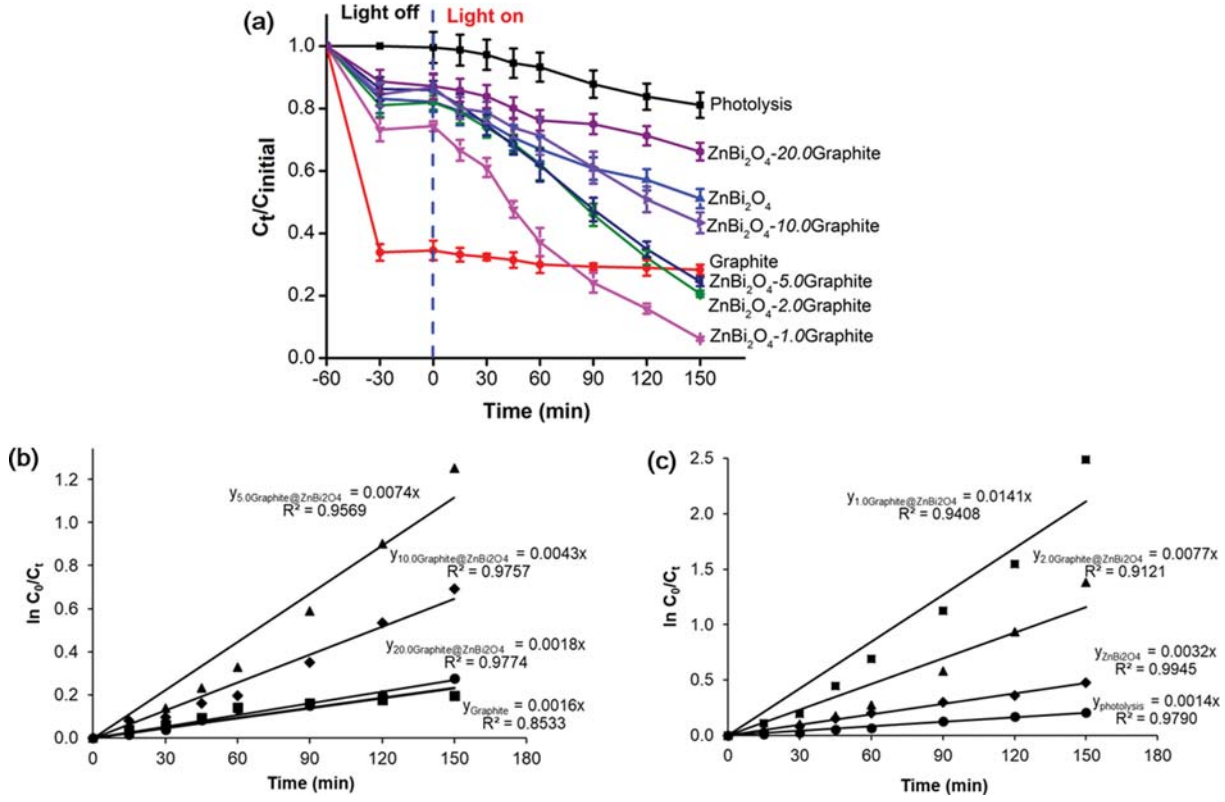

Fig. 4. (a) Photodegradation and (b) & (c) Linear kinetic degradation of RhB using $ZnBi_2O_4$-*x*Graphite catalysts under visible light irradiation.

in the $ZnBi_2O_4$-*x*Graphite catalysts at the initial stage, before and after light irradiation was measured to evaluate the photocatalytic activity of the $ZnBi_2O_4$-*x*Graphite catalysts under visible light. The results are shown in Table S2. While pristine graphite was able to remove 71.8% of RhB (Table S1), only 13.6% of TOC was removed (Table S2). This indicates that pristine graphite has a high ability for adsorption but low photocatalytic activity. The low photocatalytic activity of pristine graphite may be attributed to the fact that graphite is unable to generate sufficient active radicals under visible light. As seen in Tables S1 and S2, total RhB removal by $ZnBi_2O_4$-*1.0*Graphite was 93.8%, whereas TOC removal reached 77.7% after visible-light irradiation for 150 min, which confirmed the excellent mineralization performance of this composite under visible light. The difference in the TOC adsorbed on the $ZnBi_2O_4$-*x*Graphite catalysts before and after visible-light irradiation indicates that desorption occurred during photodegradation. Approximately 9.7 mg/L of TOC (~27.0%) was absorbed by $ZnBi_2O_4$-*1.0*Graphite before visible-light irradiation, and only ~0.8 mg/L of TOC (~2.2%) remained after visible-light irradiation for 150 min (Table S2). Thus, $ZnBi_2O_4$-*1.0*Graphite was almost free from RhB after visible-light irradiation for 150 min.

Generally, the degradation/mineralization of photocatalysts is mainly determined by the separation and recombination rates of the photogenerated electrons and holes in the photocatalysts. The hybridization of $ZnBi_2O_4$ with graphite plays a critical role in the photocatalytic efficiency, and this may be attributed to the synergetic effect of chemical contact and electron transport between $ZnBi_2O_4$ and graphite. The improvements in the photocatalytic properties of $ZnBi_2O_4$-*1.0*Graphite are mainly due to the strong electronic coupling between $ZnBi_2O_4$ and graphite, which induces spatial separation between the photoinduced e^- and h^+, and the ability of graphite to act as an electron acceptor.

A few studies have reported the degradation of RhB by different catalysts. For instance, it has been reported that the $ZnBi_2O_4$-4.0C_3N_4/Vis system degraded 95% of RhB (50 mg/L) in 90 min, using 0.5 g of catalyst per liter of solution [2]. The heterostructured 2%Bi_2S_3-$Bi_2Sn_2O_7$ composite degraded 94.4% of RhB (5 mg/L) after 360 min [8]. The nanocomposite $Bi_2Sn_2O_7$-reduced graphene oxide has also been tested, and was able to degrade 95.8% of RhB (10 mg/L) after 125 min [57]. The catalytic degradation of RhB (10 mg/L) using the Bi_2S_3-BiOCl/Vis system was 98% within 120 min [10,45]. The mineralization performance of the K(0.07)-CN [58] and CN-MoS_2-GO [7] under visible light was about 40.0 and 33.2% of 10 mg/L of RhB after 120-150 min, respectively. The photocatalyst $ZnBi_2O_4$-4.0C_3N_4/Vis system mineralized about 80% of RhB (50 mg/L) after 90 min [2].

The RhB degradation follows typical first-order kinetics, which can be expressed by $\ln(C_0/C_t)=kt$, where t is reaction time (min), k is the apparent rate constant (min^{-1}), and C_0 and C are the RhB concentrations (mmol/L) at time t=0 and t=t, respectively. The linear

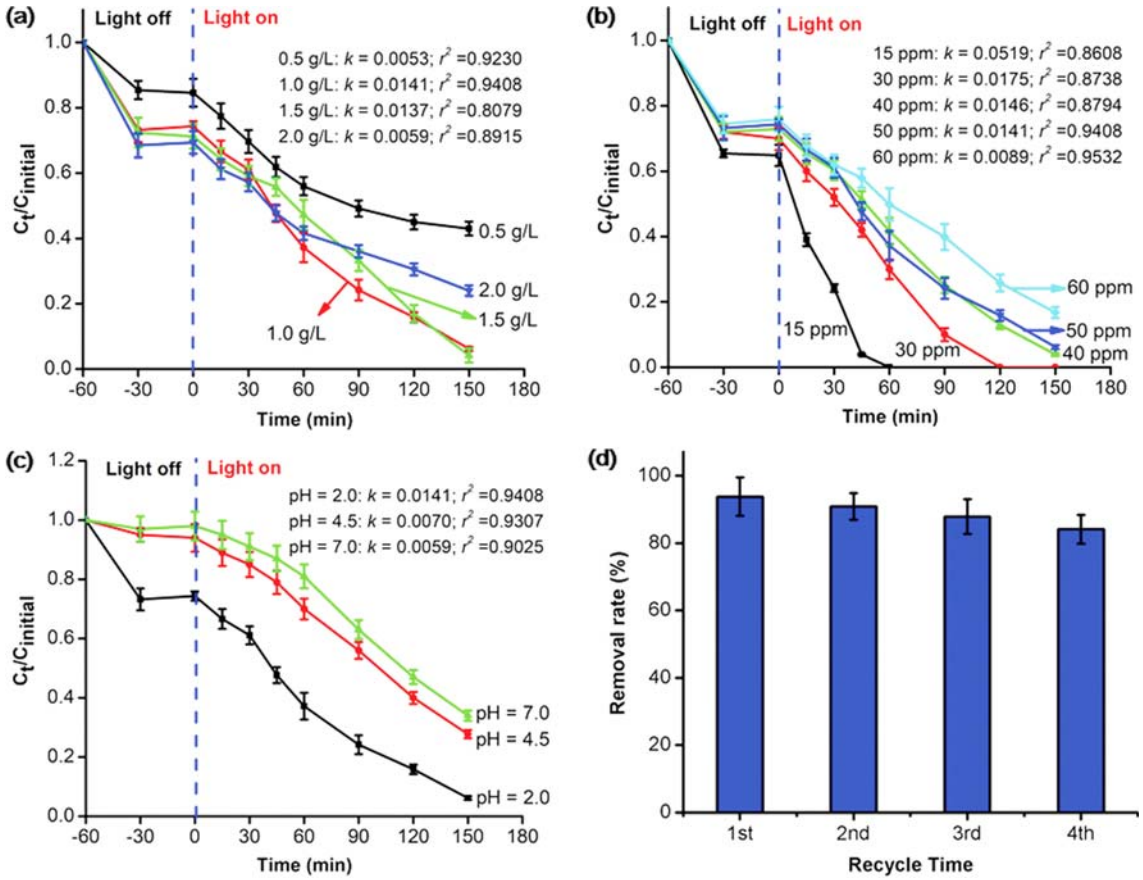

Fig. 5. Photodegradation of RhB over $ZnBi_2O_4$-*1.0*Graphite under visible light (a) effect of the loading of $ZnBi_2O_4$-*1.0*Graphite, (b) effect of initial RhB concentration, (c) Effect of pH solution, and (d) Reusability of $ZnBi_2O_4$-*1.0*Graphite catalyst under visible light.

kinetic degradation and rate constants k of RhB using the $ZnBi_2O_4$-*x*Graphite catalysts under visible-light irradiation are given in Figs. 4(b) and 4(c).

The kinetic data of the photodegradation were a good approximation to pseudo-first-order kinetic behavior (r^2=0.9121-0.9945). The order of the RhB degradation rate for as-prepared photocatalysts was $ZnBi_2O_4$-*1.0*Graphite (0.0141 min^{-1})>$ZnBi_2O_4$-*2.0*Graphite (0.0077 min^{-1})>$ZnBi_2O_4$-*5.0*Graphite (0.0074 min^{-1})>$ZnBi_2O_4$-*10.0*Graphite (0.0043 min^{-1})>$ZnBi_2O_4$ (0.0032 min^{-1})>$ZnBi_2O_4$-*20.0*Graphite (0.0018 min^{-1}). The higher the k value, the better the photocatalytic efficiency. In this study, the $ZnBi_2O_4$-*1.0*Graphite heterostructure exhibited the highest visible-light photocatalytic activity for RhB degradation. The photodegradation rate of RhB on $ZnBi_2O_4$-*1.0*Graphite was significantly higher (~4.5-fold) than that of pristine $ZnBi_2O_4$. It is obvious that the amount of graphite significantly affected the photocatalytic activity of $ZnBi_2O_4$-*x*Graphite. Thus, the incorporation of 1% of graphite into the $ZnBi_2O_4$ structure increased the rate of RhB oxidation in comparison with pristine $ZnBi_2O_4$. However, the photocatalytic activity of $ZnBi_2O_4$-*x*Graphite decreased with further increase in the graphite content. While graphite benefits charge transfer at the heterojunction interfaces, too much graphite may affect the quality of the effective heterointerfaces in $ZnBi_2O_4$-*x*Graphite [6]. In addition, excessive graphite may act as a mediator for the recombination of photoinduced e^- and h^+, ultimately reducing the photocatalytic activity [8,54].

2-1. Effect of the Loading of $ZnBi_2O_4$-*1.0*Graphite

The initial catalyst concentration dependence on RhB degradation was studied in the concentration range 0.5-2.0 g/L. Fig. 5(a) illustrates the degradation of 50 mg/L of RhB under visible-light irradiation with various loads of $ZnBi_2O_4$-*1.0*Graphite at pH 2.0. The addition of $ZnBi_2O_4$-*1.0*Graphite significantly enhanced the degradation of RhB by acting like a peroxidase-like catalyst to accelerate the generation of strong oxidizing radical species. The linear kinetic degradation of RhB is shown in Fig. S1(a). When the concentration of $ZnBi_2O_4$-*1.0*Graphite was increased from 0.5 to 1.0 g/L, the rate constant k of RhB degradation increased significantly from 0.0053 to 0.0141 min^{-1} (Fig. 5(a)). Beyond the $ZnBi_2O_4$-*1.0*Graphite loading of 1.0 g/L, the value of k decreased (0.0137-0.0059 min^{-1}), which may be due to the excessive catalyst causing opacity of the solution, thereby hindering light passing through the solution and consequently interfering with the RhB degradation reaction.

2-2. Effect of Initial RhB Concentration

The effect of initial RhB concentration on the degradation kinetics was investigated in range 15-60 mg/mL. Fig. 5(b) illustrates the degradation of RhB over $ZnBi_2O_4$-*1.0*Graphite under visible-light irradiation by varying the concentration of RhB (1.0 g/L of $ZnBi_2O_4$-*1.0*Graphite at pH 2.0). The linear kinetic degradation of RhB is shown in Fig. S1(b). It can be seen that the rate constant k of RhB degradation is greatly decreased from 0.0519 to 0.0089 min^{-1} with the increasing initial RhB concentration from 15 to 60 mg/L. This might be explained by the fact that a high concentration of RhB lowered the penetration of photons into the solution and this consequently decreased the photodegradation efficiency.

2-3. Effect of pH Solution

The effect of pH on RhB degradation over $ZnBi_2O_4$-*1.0*Graphite was investigated at different initial solution pH values (pH 2.0, 4.5, and 7.0). Fig. 5(c) shows that the maximum degradation of 50 mg/L of RhB over $ZnBi_2O_4$-*1.0*Graphite was more than 93% for a duration of 150 min at pH 2.0 (k=0.0141), while ~72% and 66% of RhB was degraded at pH 4.5 (k=0.0070) and pH 7.0 (k=0.0059), respectively. It is well-known that the acid dissociation constant pK_a of RhB is 3.1 and a change in pH results in the formation of different ionic species of RhB [59]. When pH<pKa, the carboxyl group of RhB is completely protonated (Fig. S2(a), Supporting Information). Moreover, the interaction of RhB and the surface of $ZnBi_2O_4$-*1.0*Graphite is controlled largely by electrostatic attraction or repulsion between the RhB form in solution and the surface of the $ZnBi_2O_4$-*1.0*Graphite composite. Cationic RhB predominates at pH<3, and as the surface of $ZnBi_2O_4$-*1.0*Graphite has a large number of negatively charged sites, it leads to the more cationic RhB readily undergoing photodegradation. The decreasing photodegradation of RhB at pH>3 might be due to the zwitterionic form of RhB (Fig. S2(b)). In the zwitterionic form, the attractions between the carboxyl group and xanthene groups of RhB monomers resulted in the formation of RhB dimers, making the contact between RhB and $ZnBi_2O_4$-*1.0*Graphite more difficult, and hence decreasing the degradation of RhB.

2-4. Stability and Reusability of $ZnBi_2O_4$-*1.0*Graphite

For the purpose of practical implementation, it was necessary to evaluate the stability and reusability of the $ZnBi_2O_4$-*1.0*Graphite catalyst. Experiments to determine the reusability of the catalyst in the photodegradation of the RhB solution were carried out with an initial RhB concentration of 50 mg/L at pH 2.0, and with a solid/liquid ratio of 1.0 g/L. After visible-light irradiation for 150 min, the solution was discolored. The catalyst was separated by centrifugation and then added to a fresh 50 mg/L solution of RhB under similar conditions as above. The process was repeated four times. As shown in Fig. 5(d), $ZnBi_2O_4$-*1.0*Graphite exhibited high photochemical stability, even though the photocatalyst had been recycled four times successively. This implied that the progressive reduction after fourth consecutive cycles was very small. Approximately 84.14% of RhB had been successfully degraded after four runs, indicating that the loss in photocatalytic performance of $ZnBi_2O_4$-*1.0*Graphite was insignificant after four recycling runs.

3. Photocatalytic Mechanism

It is well known that the photodegradation of organic compounds by an inorganic photocatalyst can be ascribed to different reaction pathways dominated by several active species such as •OH, $•O_2^-$, and holes (h^+) [60]. To understand the reaction mechanisms, four scavengers were used to identify the active species in the photocatalytic process. *Tert*-butanol ($C_9H_{10}O$, 2 mmol/L) as a $OH^•$ radical scavenger, *p*-benzoquinone ($C_6H_4O_2$, 2 mmol/L) as a superoxide anion radical scavenger, disodium ethylenediamine tetraacetate (EDTA-Na_2, 1 mmol/L) as a hole scavenger, or silver nitrate ($AgNO_3$, 1 mmol/L) as an electron scavenger, were added to the solution. As shown in Fig. 6(a), the photodegradation of RhB was apparently restrained after the injection of Na_2EDTA (a scavenger of h^+). The rate constant (k) was reduced from 0.0141 min^{-1} to 0.0013 min^{-1} in the photocatalytic system without any scavengers when h^+ were removed (Fig. 6(b)). The more the k value is reduced, the more important the role of the corresponding oxidative species in the reaction. Indeed, in the presence of Na_2EDTA,

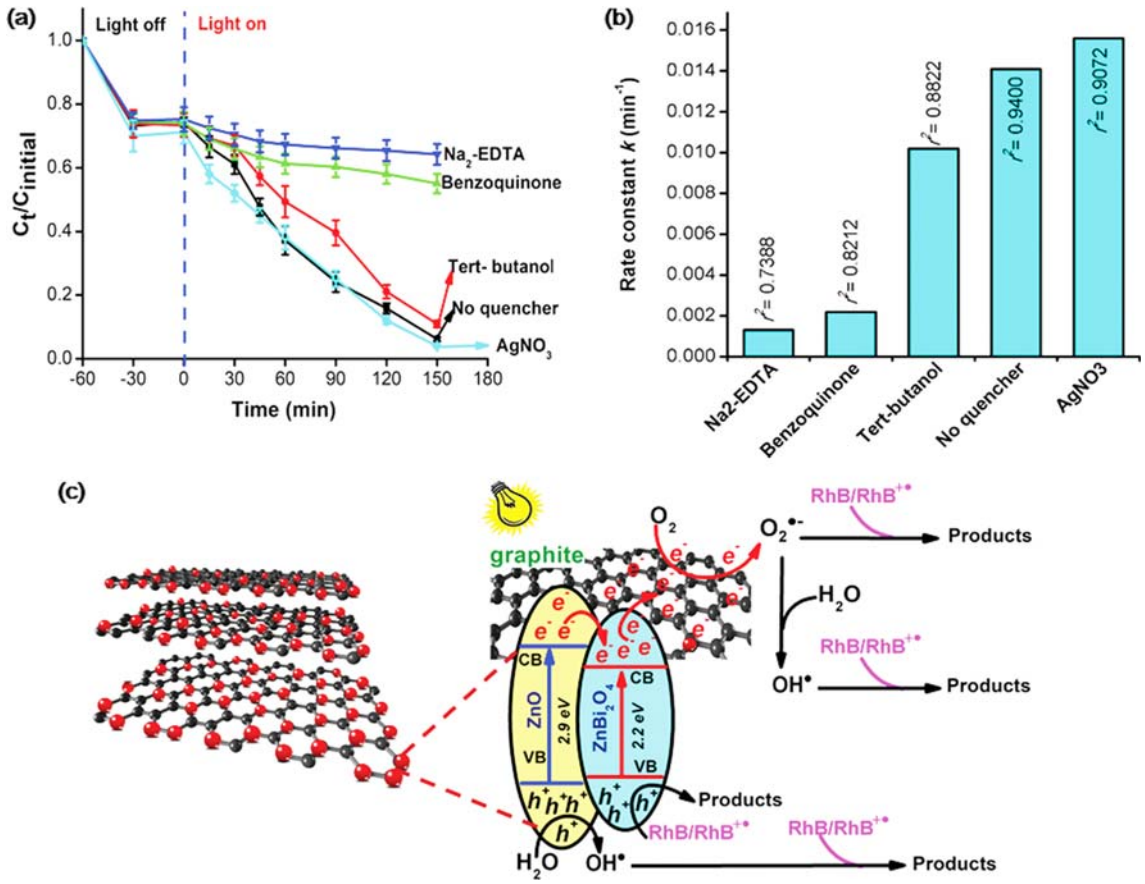

Fig. 6. (a) Photodegradation of RhB and (b) The rate constant k of photodegradation of RhB over $ZnBi_2O_4$-*1.0*Graphite under visible light with addition of h^+; e^-; $O_2^{\bullet-}$ and OH• radical scavengers and (c) The mechanisms of the RhB photodegradation over $ZnBi_2O_4$-*1.0*Graphite under visible light.

only 36% of RhB was degraded after 150 min. This result is consistent with the results reported by Zhang et al. [61] and contrary to the results obtained in other studies [6,58]. The addition of *p*-benzoquinone (a scavenger of $O_2^{\bullet-}$) caused a moderate change in the photocatalytic degradation of RhB, and approximately 45% of RhB photodegradation took place. In contrast, the addition of *tert*-butanol as a scavenger of hydroxyl radicals (OH) had a small effect on the degradation rate of RhB (k=0.0102 min^{-1}) compared to the case without a scavenger. Interestingly, the RhB photocatalytic degradation rate constant increased to 0.0156 min^{-1} when $AgNO_3$ was injected into the RhB solution to trap e^-, which is a higher rate constant than that achieved without scavengers (Fig. 6(b)). These results indicate that h^+ and $O_2^{\bullet-}$ are the major active species responsible for the complete photocatalytic mineralization of RhB, whereas the contribution of the OH• radicals is minor.

The combination of $ZnBi_2O_4$ with graphite to form the $ZnBi_2O_4$-*1.0*Graphite composite semiconductor system not only separated the photogenerated e^--h^+ pairs but also generated the photodegradation site. Pristine $ZnBi_2O_4$ was also excited and produced photogenerated e^--h^+ pairs under visible-light irradiation. As seen in Fig. 6(c), the excited state e^- was generated in the CB of $ZnBi_2O_4$ and could be directly transferred to graphite through its alternate conjugation, whereas photogenerated h^+ accumulated on the VB of $ZnBi_2O_4$. The adsorption of RhB on the $ZnBi_2O_4$-*1.0*Graphite surface is degraded by direct photogenerated h^+ oxidation. Under visible-light irradiation, RhB was transformed into its excited state (RhB*) and then the electrons were injected from RhB* into $ZnBi_2O_4$-*1.0*Graphite to form RhB$^{+\bullet}$ [6]. Oxygen adsorbed on $ZnBi_2O_4$-*1.0*Graphite reacted with the photogenerated e^- from graphite to form $O_2^{\bullet-}$. The formed $O_2^{\bullet-}$ radical could efficiently degrade RhB/RhB$^{+\bullet}$ into CO_2 and water. The photoinduced h^+ of $ZnBi_2O_4$ were able to oxidize the H_2O molecules adsorbed onto $ZnBi_2O_4$-*1.0*Graphite to OH•. As a result of charge transportation, the graphite component in $ZnBi_2O_4$-*1.0*Graphite served as a sink for the photo-excited electrons. Hence, graphite was a good candidate as an electron-attracting reservoir for photocatalytic organic pollutant degradation.

The mechanism for photodegradation of RhB by the $ZnBi_2O_4$-*1.0*Graphite catalyst under visible-light irradiation can be described by the following reactions:

$$ZnBi_2O_4 + h\nu \rightarrow ZnBi_2O_4\ (e^-, h^+) \quad (3)$$

$$RhB + h\nu \rightarrow RhB^{+\bullet} + e^- \quad (4)$$

$$ZnBi_2O_4\ (h^+) + RhB/RhB^{+\bullet} \rightarrow \text{degradation products} \rightarrow CO_2 + H_2O \quad (5)$$

$$\text{Graphite} + e^- \rightarrow \text{Graphite}\ (e^-) \quad (6)$$

$$\text{Graphite } (e^-) + O_2 \rightarrow O_2^{\bullet -} \quad (7)$$

$$O_2^{\bullet -} + \text{RhB/RhB}^{+\bullet} \rightarrow \text{degradation products} \rightarrow CO_2 + H_2O \quad (8)$$

$$O_2^{\bullet -} + 2H_2O \rightarrow 2OH^{\bullet} + 2OH^- \quad (9)$$

$$ZnBi_2O_4\ (h^+) + 2H_2O \rightarrow OH^{\bullet} + H^+ \quad (10)$$

$$OH^{\bullet} + \text{RhB/RhB}^{+\bullet} \rightarrow \text{degradation products} \rightarrow CO_2 + H_2O \quad (11)$$

$$h^+ + e^- \rightarrow (e^-, h^+) \text{ (negligible recombination reaction)} \quad (12)$$

CONCLUSIONS

A novel $ZnBi_2O_4$-Graphite photocatalyst was synthesized by a simple one-step co-precipitation method. The photocatalytic activity of the $ZnBi_2O_4$-*1.0*Graphite/Vis system composite was greatly enhanced as compared to that of pristine $ZnBi_2O_4$, as evidenced by the 4.5-times higher photocatalytic degradation rate of RhB with the $ZnBi_2O_4$-*1.0*Graphite/Vis system in comparison to that with pristine $ZnBi_2O_4$. The result shows the excellent functionality of $ZnBi_2O_4$-*1.0*Graphite as an efficient visible-light-active photocatalyst for TOC removal (77.7% of TOC was removed in 150 min). The enhancement of photocatalytic activity of $ZnBi_2O_4$-*1.0*Graphite could be mainly attributed to the effective transfer of photogenerated e^- at the heterojunction interface of $ZnBi_2O_4$ and graphite, which reduced the recombination of the e^--h^+ pairs. A study to identify the active species indicated that h^+ and $O_2^{\bullet -}$ radicals were the major species responsible for the complete mineralization with minor contributions by $OH^{\bullet}$ radicals. Additionally, the $ZnBi_2O_4$-*1.0*graphite composite exhibited stable performance during four successive recycles. Thus, we have developed a simple, efficient, and promising photocatalyst for environmental remediation.

ACKNOWLEDGEMENTS

This research is funded by Vietnam National Foundation for Science and Technology Development (NAFOSTED) under grant number 104.05-2017.29.

SUPPORTING INFORMATION

Additional information as noted in the text. This information is available via the Internet at http://www.springer.com/chemistry/journal/11814.

REFERENCES

1. Y. Yao, J. Qin, Y. Cai, F. Wei, F. Lu and S. Wang, *Environ. Sci. Pollut. Res. Int.*, **21**, 7296 (2014).
2. B. T. Huy, C. T. B. Thao, V.-D. Dao, N. T. K. Phuong and Y.-I. Lee, *Adv. Mater. Interfaces*, **4**, 1700128 (2017).
3. Y. Li, J. Wang, H. Yao, L. Dang and Z. Li, *J. Mol. Catal. A: Chem.*, **334**, 116 (2011).
4. B. T. Huy, D.-s. Jung, N. T. Kim Phuong and Y.-I. Lee, *Chemosphere*, **184**, 849 (2017).
5. J. Zhang, Y. Jiang, W. Gao and H. Hao, *J. Mater. Sci.: Mater. Electron.*, **26**, 1866 (2015).
6. H. Wang, X. Yuan, Y. Wu, G. Zeng, X. Chen, L. Leng and H. Li, *Appl. Catal., B*, **174-175**, 445 (2015).
7. S. W. Hu, L. W. Yang, Y. Tian, X. L. Wei, J. W. Ding, J. X. Zhong and P. K. Chu, *J. Colloid Interface Sci.*, **431**, 42 (2014).
8. W. Xu, J. Fang, Y. Chen, S. Lu, G. Zhou, X. Zhu and Z. Fang, *Mater. Chem. Phys.*, **154**, 30 (2015).
9. H. Cheng, B. Huang, Y. Dai, X. Qin and X. Zhang, *Langmuir*, **26**, 6618 (2010).
10. S. Jiang, K. Zhou, Y. Shi, S. Lo, H. Xu, Y. Hu and Z. Gui, *Appl. Surf. Sci.*, **290**, 313 (2014).
11. J. Cao, B. Xu, H. Lin, B. Luo and S. Chen, *Catal. Commun.*, **26**, 204 (2012).
12. Y. Cui, Q. Jia, H. Li, J. Han, L. Zhu, S. Li, Y. Zou and J. Yang, *Appl. Surf. Sci.*, **290**, 233 (2014).
13. M. Yan, Y. Wu, Y. Yan, X. Yan, F. Zhu, Y. Hua and W. Shi, *ACS Sustainable Chem. Eng.*, **4**, 757 (2016).
14. G. Zhang, B. Lin, W. Yang, S. Jiang, Q. Yao, Y. Chen and B. Gao, *RSC Adv.*, **5**, 5823 (2015).
15. R. Ma, L. Dong, B. Li, T. Su, X. Luo, Z. Qin and H. Ji, *ChemistrySelect*, **3**, 5891 (2018).
16. P. Du, T. Su, X. Luo, X. Zhou, Z. Qin, H. Ji and J. Chen, *Chin. J. Chem.*, **36**, 538 (2018).
17. T. Su, R. Peng, Z. D. Hood, M. Naguib, I. N. Ivanov, J. K. Keum, Z. Qin, Z. Guo and Z. Wu, *ChemSusChem.*, **11**, 688 (2018).
18. T. Su, Q. Shao, Z. Qin, Z. Guo and Z. Wu, *ACS Catalysis*, **8**, 2253 (2018).
19. S. Xia, L. Zhang, X. Zhou, M. Shao, G. Pan and Z. Ni, *Appl. Catal., B*, **176-177**, 266 (2015).
20. Y.-F. Chao, P.-C. Chen and S.-L. Wang, *Appl. Clay Sci.*, **40**, 193 (2008).
21. N. K. Lazaridis, T. D. Karapantsios and D. Georgantas, *Water Res.*, **37**, 3023 (2003).
22. I. Pavlovic, C. Barriga, M. C. Hermosín, J. Cornejo and M. A. Ulibarri, *Appl. Clay Sci.*, **30**, 125 (2005).
23. J. Inacio, C. Taviot-Guého, C. Forano and J. P. Besse, *Appl. Clay Sci.*, **18**, 255 (2001).
24. G. Jale, A. Zehra and Ö. Mahmure, *Am. J. Eng. Res.*, **2**, 1 (2013).
25. L. Shao, Y. Yao, S. Quan, H. Wei, R. Wang and Z. Guo, *Mater. Lett.*, **114**, 111 (2014).
26. A. Mantilla, F. Tzompantzi, J. L. Fernández, J. A. I. Díaz Góngora, G. Mendoza and R. Gómez, *Catal. Today*, **148**, 119 (2009).
27. J. S. Valente, F. Tzompantzi, J. Prince, J. G. H. Cortez and R. Gomez, *Appl. Catal., B*, **90**, 330 (2009).
28. X. Xiang, F. Li and Z. Huang, *Rev. Adv. Sci. Eng.*, **3**, 158 (2014).
29. N. T. K. Phuong, *Environ. Technol.*, **35**, 2829 (2014).
30. H. N. N. Ha, N. T. K. Phuong, T. Boi An, N. T. M. Tho, T. N. Thang, B. Q. Minh and C. V. Du, *J. Environ. Sci. Health, Part A: Environ. Sci. Eng.*, **51**, 403 (2016).
31. H. N. N. Ha, N. T. K. Phuong and N. T. M. Tho, *Desalination Water Treatment*, **57**, 27741 (2016).
32. S. P. Paredes, M. A. Valenzuela, G. Fetter and S. O. Flores, *J. Phys. Chem. Solids*, **72**, 914 (2011).
33. E. Dvininov, M. Ignat, P. Barvinschi, M. A. Smithers and E. Popovici, *J. Hazard. Mater.*, **177**, 150 (2010).
34. J. S. Valente, F. Tzompantzi and J. Prince, *Appl. Catal., B*, **102**, 276 (2011).

35. E. Martín del Campo, J. S. Valente, T. Pavón, R. Romero, Á. Mantilla and R. Natividad, *Ind. Eng. Chem. Res.*, **50**, 11544 (2011).
36. Z. Huang, P. Wu, Y. Lu, X. Wang, N. Zhu and Z. Dang, *J. Hazard. Mater.*, **246**-**247**, 70 (2013).
37. R. Lu, X. Xu, J. Chang, Y. Zhu, S. Xu and F. Zhang, *Appl. Catal., B*, **111**-**112**, 389 (2012).
38. X. Xu, R. Lu, X. Zhao, S. Xu, X. Lei, F. Zhang and D. G. Evans, *Appl. Catal., B*, **102**, 147 (2011).
39. G. Mendoza-Damián, F. Tzompantzi, A. Mantilla, A. Barrera and L. Lartundo-Rojas, *J. Hazard. Mater.*, **263**, Part 1, 67 (2013).
40. N. Wang, L. Zhu, Y. Huang, Y. She, Y. Yu and H. Tang, *J. Catal.*, **266**, 199 (2009).
41. X. Xiang, L. Xie, Z. Li and F. Li, *Chem. Eng. J.*, **221**, 222 (2013).
42. N. T. Kim Phuong, M.-w. Beak, B. T. Huy and Y.-I. Lee, *Chemosphere*, **146**, 51 (2016).
43. L. Mohapatra and K. Parida, *J. Mater. Chem. A*, **4**, 10744 (2016).
44. L. Mohapatra and K. M. Parida, *Phys. Chem. Chem. Phys.*, **16**, 16985 (2014).
45. Y. Zhu, P. Wu, S. Yang, Y. Lu, W. Li, N. Zhu, Z. Dang and Z. Huang, *RSC Adv.*, **6**, 37689 (2016).
46. M. Shao, J. Han, M. Wei, D. G. Evans and X. Duan, *Chem. Eng. J.*, **168**, 519 (2011).
47. L. Mohapatra and K. M. Parida, *Sep. Purif. Technol.*, **91**, 73 (2012).
48. K. M. Parida and L. Mohapatra, *Chem. Eng. J.*, **179**, 131 (2012).
49. C. Li, Y. Dong, J. Yang, Y. Li and C. Huang, *J. Mol. Liq.*, **196**, 348 (2014).
50. J. Jia, D. Li, J. Wan and X. Yu, *J. Ind. Eng. Chem.*, **33**, 162 (2016).
51. G. Palmisano, V. Loddo, H. H. E. Nazer, S. Yurdakal, V. Augugliaro, R. Ciriminna and M. Pagliaro, *Chem. Eng. J.*, **155**, 339 (2009).
52. T. Ndlovu, A. T. Kuvarega, O. A. Arotiba, S. Sampath, R. W. Krause and B. B. Mamba, *Appl. Surf. Sci.*, **300**, 159 (2014).
53. K. Dědková, J. Lang, K. Matějová, P. Peikertová, J. Holešinský, V. Vodárek and J. Kukutschová, *J. Photochem. Photobiol., B*, **149**, 265 (2015).
54. S. Nayak, L. Mohapatra and K. Parida, *J. Mater. Chem. A*, **3**, 18622 (2015).
55. V. B. R. Boppana and R. F. Lobo, *ACS Catalysis*, **1**, 923 (2011).
56. N. Wu, X. She, D. Yang, X. Wu, F. Su and Y. Chen, *J. Mater. Chem.*, **22**, 17254 (2012).
57. H. Liu, Z. Jin, Y. Su and Y. Wang, *Sep. Purif. Technol.*, **142**, 25 (2015).
58. S. Hu, F. Li, Z. Fan, F. Wang, Y. Zhao and Z. Lv, *Dalton Trans.*, **44**, 1084 (2015).
59. I. L. Arbeloa and K. K. Rohatgi-Mukherjee, *J. Hazard. Mater.*, **128**, 474 (1986).
60. Y. Qu and X. Duan, *Chem. Soc. Rev.*, **42**, 2568 (2013).
61. S. Zhang, Y. Yang, Y. Guo, W. Guo, M. Wang, Y. Guo and M. Huo, *J. Hazard. Mater.*, **261**, 235 (2013).

Supporting Information

Facile synthesis of $ZnBi_2O_4$-graphite composites as highly active visible-light photocatalyst for the mineralization of rhodamine B

Nguyen Thi Mai Tho[*,**], Bui The Huy[**,*******,†], Dang Nguyen Nha Khanh[***], Ho Nguyen Nhat Ha[***], Vu Quang Huy[***], Ngo Thi Tuong Vy[*****], Do Manh Huy[******], Duong Phuoc Dat[******], and Nguyen Thi Kim Phuong[*,***,†]**

*Graduate University of Science and Technology, Vietnam Academy of Science and Technology (VAST), 18 Hoang Quoc Viet, Cau Giay, Hanoi, Vietnam
**Institute of Research and Development, Duy Tan University, 03 Quang Trung, Da Nang, Vietnam
***HoChiMinh City Institute of Resources Geography, VAST, 01 Mac Dinh Chi, Ho Chi Minh City, Vietnam
****Chemical Engineering Faculty - Industrial University of Ho Chi Minh City, Vietnam
*****University of Science, National University of Ho Chi Minh City, Vietnam
******Institute of Chemical Technology, VAST, 01 Mac Dinh Chi, Ho Chi Minh City, Vietnam
*******Department of Chemistry, Changwon National University, Changwon 51140, Korea
(*Received 22 April 2018 • accepted 27 September 2018*)

EXPERIMENTAL

1. Equipments

XRD measurements were performed by using a Rigaku Ultima IV X-ray diffractometer (Japan). The patterns with Cu Kα radiation (λ= 1.54051 Å) at 40 kV and 40 mA were recorded with 2θ ranging from 10° to 70°. SEM micrographs were examined using a Tescan MIRA-3 LM scanning electron microscope (U.S.) with an accelerating voltage of 20 kV. Zn and Bi element analysis was conducted using inductively coupled plasma (ICP) emission spectroscopy on a Perkin-Elmer Optima 5000DV instrument. The UV-Vis diffuse reflectance spectrum (DRS) was recorded on a Jasco V670 UV-Vis spectrophotometer (Japan) with an integrating sphere attachment. The liquid total organic carbon (TOC) of samples was determined with a Shimadzu TOC-VCPH analyzer (Japan). The concentration of rhodamine B was monitored by measuring the UV-Vis spectra using a Thermo Evolution 201 UV-Visible spectrophotometer (U.S.).

To calculate the TOC removal (%), the following equation was used:

Table S1. The results of adsorption and total RhB removal using graphite, $ZnBi_2O_4$, $ZnBi_2O_4$-*x*Graphite (reaction condition: 100 mL RhB 50 mg/L, 0.1 g catalyst, pH 2.0)

As-prepared samples	Adsorption (%)*	Total removal (%)**
Graphite	65.5	71.8
$ZnBi_2O_4$	17.9	48.9
$ZnBi_2O_4$-*1.0*Graphite	**25.7**	**93.8**
$ZnBi_2O_4$-*2.0*Graphite	18.1	79.4
$ZnBi_2O_4$-*5.0*Graphite	14.1	75.5
$ZnBi_2O_4$-*10.0*Graphite	13.2	56.6
$ZnBi_2O_4$-*20.0*Graphite	12.8	33.8

*After 60 min dark adsorption
**After 150 min visible light irradiation

$$TOC_{removal}(\%) = \frac{TOC_{in} - TOC_{re}}{TOC_{in}} \times 100 \quad (1)$$

where TOC_{in} (mg) refer to the initial TOC values; TOC_{re} (mg) refer

Table S2. Amount of TOC in solution and on graphite, $ZnBi_2O_4$, $ZnBi_2O_4$-*x*Graphite (reaction condition: 100 mL of RhB 50 mg/L, 0.1 g catalyst, pH 2.0)

As-prepared samples	TOC in solution (mg TOC/L solution)			TOC in as-prepared samples (mg TOC/1.0 g catalyst)		Total TOC removed	
	Initial	Before irradiation	After irradiation	Before irradiation	After irradiation	(mg)	%
Graphite		12.2±0.9	11.5±0.4	23.4±0.5	19.2±0.6	4.9	13.6
$ZnBi_2O_4$		29.8±0.4	20.1±0.9	6.8±0.6	1.7±0.2	14.8	41.2
$ZnBi_2O_4$-*1.0*Graphite		**26.8±0.5**	**7.8±0.2**	**9.7±0.6**	**0.8±0.3**	**27.9**	**77.7**
$ZnBi_2O_4$-*2.0*Graphite	35.9±0.8	30.1±0.4	11.2±0.8	6.8±0.5	1.3±0.4	24.4	68.0
$ZnBi_2O_4$-*5.0*Graphite		31.3±0.6	13.3±0.7	4.9±0.3	1.4±0.3	21.5	59.9
$ZnBi_2O_4$-*10.0*Graphite		31.6±0.4	16.9±0.4	4.8±0.4	1.6±0.2	17.9	49.9
$ZnBi_2O_4$-*20.0*Graphite		30.9±0.7	24.2±0.5	4.9±0.6	1.8±0.3	9.8	27.3

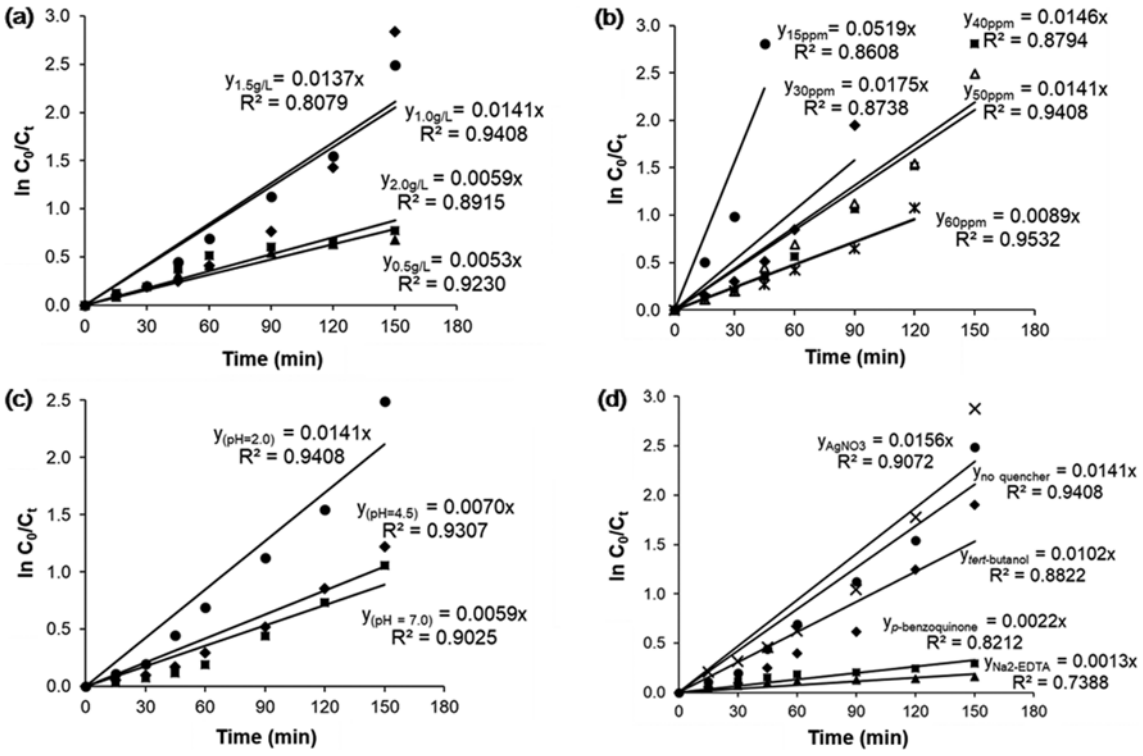

Fig. S1. Linear kinetic degradation of RhB under visible light over $ZnBi_2O_4$-*1.0*Graphite (a) effect of the loading of $ZnBi_2O_4$-*1.0*Graphite; (b) effect of initial RhB concentration; (c) effect of pH solution (d) effect of addition of e^-; h^+; $O_2^{\bullet-}$ and $OH^\bullet$ radical scavengers.

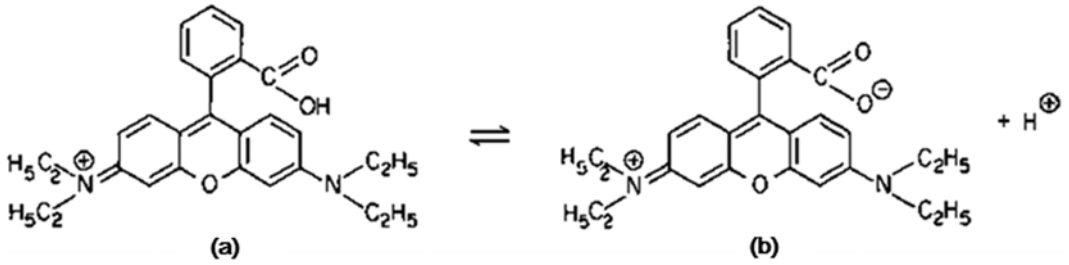

Fig. S2. Dissociation equilibrium of RhB in aqueous solution (a) cationic form (b) zwitterionic form (acid dissociation constant of RhB, pK_a=3.1).

to the remaining TOC in solution and on $ZnBi_2O_4$-*12.0*Bi_2S_3 after visible light irradiation.